Dalton Transactions

ROYAL SOCIETY OF CHEMISTRY

COMMUNICATION

View Article Online
View Journal | View Issue

Cite this: *Dalton Trans.*, 2025, **54**, 17772

Received 27th October 2025,
Accepted 21st November 2025

DOI: 10.1039/d5dt02573g

rsc.li/dalton

Oxidation-induced irreversible phase transformation of ethyltriphenylphosphonium-based copper chloride single crystals for achieving second harmonic generation and magnetism

Mengjie Sang,[a] Yanqing Liu,*[a] Guokui Liu [b] and Yangyang Dang *[a]

The irreversible transformation of $ETPCuCl_2$ into $ETPCuCl_3$ achieves functional switching from second harmonic generation to magnetism through an oxidation-induced phase transformation strategy, which not only offers a new approach to the design of novel multifunctional materials, but also guides applications in optical and spintronic devices.

Phase transformation is essentially a process of structural performance synergy changes between different phases caused by external environmental influences, such as temperature, solvent atmosphere, light, pressure, electric field, chemical environment, pH regulation, selective solvent induction, and chiral ligand induction. Among these, oxidation-induced phase transformation (OIPT), as a typical chemically driven phase transformation process, is an irreversible process between different valence states of metals,[1] including $Cu^{+} \rightarrow Cu^{2+}$, $Ti^{3+} \rightarrow Ti^{4+}$, $Sn^{2+} \rightarrow Sn^{4+}$, $V^{4+} \rightarrow V^{5+}$, $Mn^{2+} \rightarrow Mn^{4+}$, *etc.*,[2–6] which amplifies the small electronic structure changes of atoms into changes in crystal symmetry, dimensional characteristics, and material properties. The phase transformation of materials is also a method for preparing new substances to achieve a wider range of applications, and it has become a research hotspot in fields such as light-emitting devices, sensors,[7–9] information storage,[10–12] catalysis,[13,14] biomedicine, energy conversion, and gas storage. Organic–inorganic hybrid metal halides are a type of functional material formed by the coordination or ionic bonding of metal halide anion frameworks with organic/inorganic cations, possessing a diversity of metal valence states and a wide range of structures, which are an ideal platform for investigating phase transformations.[15,16] Compared to other organic–inorganic hybrid metal halides, the advantages of copper-based hybrid materials lie in their excellent cost-effectiveness and sustainability, combined with their unique chemical properties, such as variable valence state, flexible coordination, catalytic performance, and efficient luminous ability. Moreover, copper-based hybrid materials serve as an ideal model system for elucidating the fundamental mechanisms of OIPT due to their unique multi-valent coordination characteristics (Cu^{+}/Cu^{2+}). For example, the $Cu^{+} \rightarrow Cu^{2+}$ valence transition readily occurs in an oxidizing environment, which can alter the symmetry of the coordination polyhedron through changes in the Cu–O bond length and drive the crystal to undergo structural reconstruction from a low-dimensional chain-like structure (*e.g.*, $[CuI_2]_n$) to a three-dimensional open framework structure (*e.g.*, Cu-MOF-74). In copper(I) based organic–inorganic hybrid materials, the d^{10} closed-shell electron configuration of Cu^{+} confers non-centrosymmetric bonding characteristics (linear/tetrahedral coordination), conferring unique advantages in second harmonic generation.[17–19] Owing to the Jahn–Teller effect-induced octahedral structural distortion,[20–22] the d^9 configuration of Cu^{2+} is capable of altering the crystal lattice symmetry of copper(II) based organic–inorganic hybrid materials to induce tunable absorption in the near-infrared region through d–d transition pathways and activate single-ion magnetic anisotropy. Interestingly, the accompanying magnetic ground state transition during this process is particularly important. The pristine Cu^{+} system exhibits diamagnetism due to its d^{10} unmagnetized state. In contrast, oxidized Cu^{2+} forms long-range antiferromagnetic order through superexchange interactions involving its unpaired electrons, enhancing magnetic anisotropy,[23] thereby providing a design foundation for spin valve devices. Therefore, utilizing changes in the valence of metal ions to achieve significant structural and performance changes in copper-based organic–inorganic hybrid materials has certain practical significance. Here, bulk $ETPCuCl_2$ ($ETP{=}C_{20}H_{20}P$) and $ETPCuCl_3$ single crystals were grown by the slow evaporation method, and their OIPT process was discovered for the first time. The structure of the material changes from non-centrosymmetric to centrosymmetric, accompanied by a shift in performance from frequency dou-

[a]*School of Physics and Physical Engineering, Qufu Normal University, Qufu 273165, P. R. China. E-mail: dyy@qfnu.edu.cn, yanqingliu@qfnu.edu.cn*
[b]*School of Chemistry and Chemical Engineering, Linyi University, Linyi 276000, P. R. China*

bling to magnetism. Furthermore, the in-depth exploration of structure–property correlations for $ETPCuCl_2$ and $ETPCuCl_3$ crystals induced by oxidation could not only provide a theoretical framework for designing phase-change materials, but also lay the foundation for the development of next-generation multifunctional magnetic materials.

The crystal growth strategy is shown in Scheme 1. The starting materials were ETPCl and CuCl mixed in a 1 : 1 molar ratio, which were reacted in an appropriate amount of HCl–H_3PO_2 mixed solvent. Using the slow evaporation method, two organic–inorganic hybrid halide crystals were grown: $ETPCuCl_2$ (colorless and transparent plate-like crystals, Fig. 1a) and $ETPCuCl_3$ (black bulk crystals, Fig. 1b). Notably, $ETPCuCl_2$ single crystals underwent oxidation when exposed to air in the mother liquor for approximately 3 days. The mother liquor changed from colorless and transparent to green and transparent and eventually turned into a black solution (Fig. S1, SI). This process indicated the gradual oxidation of Cu^+ to Cu^{2+} until complete oxidation, and the $ETPCuCl_3$ crystals were obtained, as shown in Fig. 1b and Fig. S2 (SI).

Oxidation-induced phase transformation is essentially a redox reaction where the oxidation states of certain elements within crystals change. These alterations in oxidation states lead to shifts in bond lengths and angles within the crystalline materials, thereby affecting their crystal structure. In the process of $ETPCuCl_2 \rightarrow ETPCuCl_3$, the core reaction equation of oxidation–reduction is $Cu^+ \rightarrow Cu^{2+} + e^-$. This process requires a suitable oxidizing reagent to accept the electron. This reaction is conducted in an acidic environment, which can facilitate the progression. In the experiment, the Cu(II) form is more stable under acidic conditions, preventing its hydrolysis into other precipitates. The oxidation process is not merely "*in situ*" oxidation, and it can cause the original cuprous-based crystal framework to fracture and reorganize, forming a new copper-based framework. At room temperature, the crystal structures of $ETPCuCl_2$ and $ETPCuCl_3$ were determined through single-crystal X-ray diffraction (SCXRD). $ETPCuCl_2$ crystals are found to belong to the monoclinic crystal system, with the space group $P2_1$ (no. 4), exhibiting a non-centrally symmetric structure. $ETPCuCl_3$ belongs to the monoclinic crystal system, with the space group $C2/c$ (no. 15), exhibiting a centrosymmetric structure, as shown in Table S1 (SI). Detailed bond length and angle data are presented in Tables S2 and S3 (SI). Surprisingly, XRD results indicate that atoms in $ETPCuCl_2$ crystals form a metal halide chain structure, resulting in a non-centrosymmetric arrangement. In contrast, the peak of the $ETPCuCl_3$ single crystal generated by Cu^{2+} oxidation crystallization shifts to the right as a whole without obvious splitting, which corresponds to the phenomenon of lattice distortion. This transformation originates from the Jahn–Teller effect, wherein asymmetric electron distribution induces crystal field distortion. This distortion influences the magnetic properties of copper ions, manifesting magnetic behavior in this structure.[22] Concurrently, Cu atoms coordinate with any four Cl atoms, forming polyhedral structural units. As shown in Fig. 1c and d, the inorganic composition of $ETPCuCl_2$ single crystals changes before and after the phase transformation. The coordination number of copper atoms shifts from 2 to 4, leading to abrupt changes in lattice parameters, bond lengths, and bond angles compared to $ETPCuCl_2$.[20,21] In Fig. 1e, powder X-ray diffraction (PXRD) patterns of $ETPCuCl_2$ and $ETPCuCl_3$ agree well with the single-crystal X-ray diffraction (SCXRD) patterns. To qualitatively analyze the chemical state of $ETPCuCl_2$ and $ETPCuCl_3$ crystal materials, XPS measurements were performed on both crystals. The test results are shown in Fig. S3 (SI). All XPS test results were calibrated based on C 1s (284.8 eV). Especially, the XPS spectrum of the Cu 2p binding energy for the $ETPCuCl_2$ single crystal exhibits a doublet, as shown in Fig. S3b, with peaks at 952 eV ($2p_{1/2}$) and 932 eV ($2p_{3/2}$), and a splitting energy of 20 eV. It should be noted that the binding energy of Cu^{2+} in the Cu 2p region typically lies around 935 eV, but no peak at this position is present in the Cu 2p spectrum, indicating the absence of Cu^{2+} in the sample. In the full XPS spectra of $ETPCuCl_3$, the presence of Cu^{2+} in the material is clearly evident, as shown in Fig. S3g (SI). Although the main XPS peak position of Cu^{2+} in Cu 2p region is similar to that of Cu^+, it typically exhibits a distinct peak in the 935 eV–940 eV range, which is used to distinguish between the two valence states. As shown in Fig. S3b (SI), a distinct peak is observed near 937 eV, confirming the presence of Cu^{2+}. Comparing the XPS spectra reveals that when the $ETPCuCl_2$ sample is exposed to air, Cu^+ is easily oxidized, with all Cu^+ being oxidized to Cu^{2+}. The bond valence sum (BVS) calculations indicate that the valence states of Cu (1.18) in $ETPCuCl_2$ and Cu (2.04) in $ETPCuCl_3$ are near +1 and +2, respectively. The details of BVS calculations are shown in Table S4 (SI).

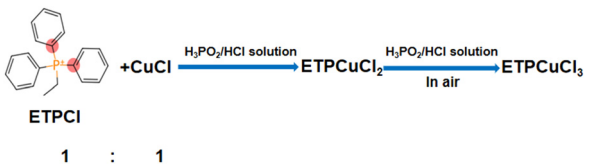

Scheme 1 Synthesis route to $ETPCuCl_2$ and $ETPCuCl_3$ by the reaction of ETPCl and CuCl raw materials.

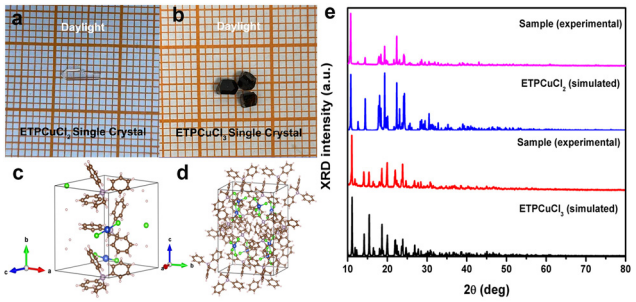

Fig. 1 Photographs, structures, and PXRD of $ETPCuCl_2$ and $ETPCuCl_3$ crystals. Photographs of $ETPCuCl_2$ (a) and $ETPCuCl_3$ (b) crystals; crystal structures of $ETPCuCl_2$ (c) and $ETPCuCl_3$ (d); (e) PXRD and SCXRD diagrams of $ETPCuCl_2$ and $ETPCuCl_3$.

Based on the aforementioned research, we conducted an in-depth study of the optical properties and band gap of the material before and after the phase transformation. The electronic properties of $ETPCuCl_2$ and $ETPCuCl_3$ were calculated using density functional theory (DFT). The UV-vis spectra results are shown in Fig. 2a and d. $ETPCuCl_2$ exhibits an optical bandgap of 3.35 eV, while the optical bandgap of $ETPCuCl_3$ is 2.09 eV. In DFT calculations, as shown in Fig. 2b and e, $ETPCuCl_2$ has a direct bandgap of 2.23 eV, with the valence band maximum (VBM) and conduction band minimum (CBM) both located at the Z point. In contrast, $ETPCuCl_3$ has an indirect bandgap of 0.36 eV, with the VBM at the Γ point and the CBM at the Z point. This indicates that the band gap decreases after the phase transformation, and the two systems align well. Additionally, we calculated the projected density of states (PDOS) plots for all studied systems and selected key components from the plots. Fig. 2c and f show that the VBM of $ETPCuCl_2$ is primarily composed of Cu 3d and Cl 3p atomic orbitals, while the CBM is primarily composed of C 2p atomic orbitals. Especially, C 2p represents the whole organic cation (ETP). In contrast, the valence band maximum (VBM) of $ETPCuCl_3$ is primarily composed of spin-up Cl 3p and Cu 3d atomic orbitals, while the conduction band minimum (CBM) is primarily composed of spin-down Cl 3p and Cu 3d atomic orbitals.

Since second harmonic generation (SHG) is a typical nonlinear optical characteristic, its essence relies on the non-centrosymmetric structure within the whole material.[24,25] This structure effectively breaks the spatial inversion symmetry, thereby achieving frequency multiplication efficiency. Based on the unique non-centrosymmetric structural characteristics of $ETPCuCl_2$ crystals, experimental investigations into their second-order nonlinear optical (NLO) properties were performed. During the experiment, potassium dihydrogen phosphate (KDP) polycrystals were selected as the reference standard for SHG signal intensity. The measurement results in Fig. 3a indicate that the SHG intensity stabilizes at approximately 0.6 times that of KDP. This result clearly demonstrates the significant second-harmonic generation effect exhibited by this crystal material, confirming its promising application in the field of nonlinear optics. Furthermore, since SHG effect in powder samples primarily depends on particle size, the $ETPCuCl_2$ crystal samples were ground and screened to obtain five distinct powder particle size ranges of 40–80, 80–100, 100–180, 180–280, and 280–460 μm. As shown in Fig. 3b, the SHG intensity exhibits an increasing trend with growing particle size. When the particle size reaches approximately 280 μm, the SHG signal intensity gradually approaches saturation. This behavior fully aligns with type I phase matching (PM) characteristics. In-depth analysis shows that the second harmonic generation effect of the $ETPCuCl_2$ crystal is attributed to the internal lattice distortion and the synergy between organic ligands and metal ions. These factors collectively contribute to the formation of the crystal's overall non-centrosymmetric structure. Traditionally, second-order nonlinear optical (NLO) and magnetic properties have been jointly determined using distinct ion/ligand designs, crystal symmetries, and electronic configurations, respectively. These two properties were considered mutually independent and mutually exclusive (strong NLO requires non-centrosymmetric crystal structures and d^0/d^{10} closed-shell electronic configurations, while magnetic properties demand open-shell electronic configurations and spin order). In this study, however, the oxidation of Cu^+ to Cu^{2+} induces a significant change in elemental valence states, leading to a transformation in the crystal material's properties and enabling a switch from second harmonic generation to magnetism.

The magnetic properties of crystalline materials primarily originate from the motion of electrons within atoms. According to quantum mechanics, this motion manifests in two forms: first, the orbital motion of electrons around the nucleus, generating orbital magnetic moments; second, the

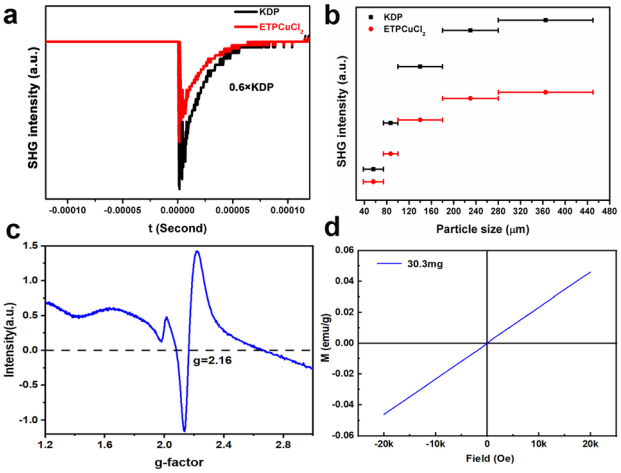

Fig. 3 (a) SHG signal of $ETPCuCl_2$ on the reference KDP with the same particle size; (b) comparison of SHG signals between $ETPCuCl_2$ and the standard material KDP with the same particle size; (c) ESR data of $ETPCuCl_3$; (d) VSM data of $ETPCuCl_3$.

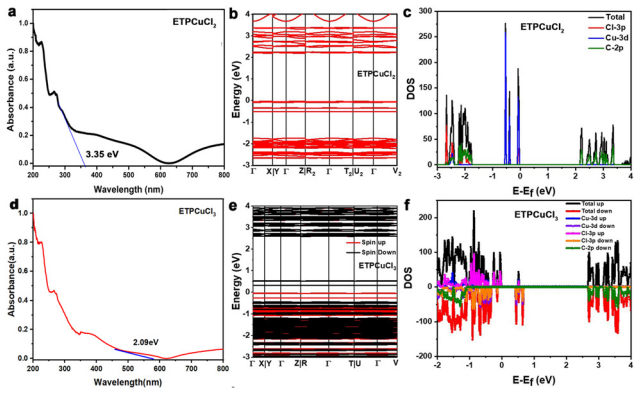

Fig. 2 (a) UV-visible diffuse reflectance spectra of $ETPCuCl_2$; (d) UV-visible diffuse reflectance spectra of $ETPCuCl_3$; (b) DFT energy band structure of $ETPCuCl_2$; (e) DFT energy band structure of $ETPCuCl_3$; (c) PDOS map of $ETPCuCl_2$; (f) PDOS map of $ETPCuCl_3$.

intrinsic spin motion of electrons, producing spin magnetic moments. Within the atomic system, these two components collectively form the total magnetic moment of the atom. At the macroscopic level of crystalline materials, magnetic properties depend on the collective ordered arrangement of atomic magnetic moments through mechanisms such as interactions. Among these, exchange interaction—a quantum mechanical force causes the magnetic moments of neighboring atoms to align either parallel (ferromagnetism) or antiparallel (antiferromagnetism), endowing materials with diverse magnetic behaviors. To elucidate the aforementioned principle, the oxidation-induced phase transition of a class of copper-based materials was studied. For instance, oxidation serves as a significant external stimulus capable of triggering pronounced phase transformations within crystalline materials. This primarily manifests as a structural transition from non-centrosymmetric to centrosymmetric crystal structures. Such a shift in symmetry directly induces a transition in material properties from second-order nonlinearity to magnetic characteristics. During this phase transformation, the fundamental cause of magnetism lies in the oxidation of Cu^{+} to Cu^{2+}.[26] At this time, the crystal structure changes to a centrosymmetric structure. This oxidation process creates magnetic moment carriers possessing unpaired electrons ($S = 1/2$ or $-1/2$). For copper ions, the electronic configuration of the Cu^{2+} ion is $3d^9$, with one unpaired electron residing in its 3d orbital. The presence of this electron constitutes the essential condition for the material to exhibit magnetism.[27,28]

To investigate the magnetic properties exhibited by $ETPCuCl_3$ crystals, this study systematically examined the regulatory effect of copper ion localization changes induced by oxidation on magnetic behavior. This was achieved through a combined approach utilizing electron paramagnetic resonance (EPR) and vibrating sample magnetometer (VSM) methods.[29–32] In the EPR measurements, the prominent resonance absorption peak observed in the spectrum (Fig. 3c) revealed a *g*-factor of 2.16 for the divalent copper crystal material. This value significantly deviates from the *g*-factor of free electrons (2.0023), directly indicating that the 3d orbital electrons of copper ions are strongly influenced by surrounding ligands. Further analysis suggests that this deviation likely stems from the crystal field effect. Specifically, copper ions interact with surrounding non-magnetic ligands (*e.g.*, chloride ions), causing splitting of the 3d electronic levels and forming orbitals with distinct energies. From an electronic structure perspective, the Cu^{2+} ion possesses a $3d^9$ configuration with one unpaired electron (spin $S = 1/2$ or $-1/2$). The crystal field effect further splits the 3d orbitals into e_g ($d_{x^2-y^2}$, d_{z^2}) and t_{2g} (d_{xy}, d_{xz}, d_{yz}) orbitals. Among these, the $d_{x^2-y^2}$ orbital energy increases due to the Jahn–Teller distortion, with the unpaired electron predominantly occupying this orbital to form an axially oriented spin state. This behaviour is consistent with the deviation of the experimental value $g = 2.16$. The single-peak characteristic of the electron paramagnetic resonance spectrum further indicates that Cu^{2+} ions within the crystal occupy a uniformly coordinated environment. Its spin–orbital coupling is mediated by the coordination field, resulting in an isotropic electron paramagnetic resonance signal. This aligns with the characteristics of a layered perovskite structure, where Cu^{2+} ions exhibit a regular in-layer arrangement.

Additionally, VSM test results serve as a crucial method for characterizing a material's magnetic properties, providing an intuitive reflection of the material's magnetization strength (M) under an external magnetic field (H). As clearly shown in the results of Fig. 3d, the divalent copper crystal material exhibits a good linear magnetization response relationship under an applied magnetic field, with no hysteresis phenomena (such as remanence or coercivity), consistent with the paramagnetic behaviour. This phenomenon originates from the magnetic moments of Cu^{2+} ions exhibiting antiferromagnetic coupling within the crystal structure. Specifically, when the bond angle approaches 90°, Cu^{2+} and Cl^{-} form a Cu–Cl–Cu bridging structure. The super-exchange interaction mediated by the non-magnetic Cl^{-} ligand is typically weak and antiferromagnetic, arising from insufficient orbital overlap.[33] At the measurement temperature, thermal kinetic energy overcomes the weak intra-layer antiferromagnetic coupling, preventing the formation of long-range magnetic order. Consequently, the system exhibits a paramagnetic linear magnetisation response rather than ferromagnetic or antiferromagnetic behaviour with hysteresis characteristics.[34] Furthermore, the spatial isolation effect of interlayer organic cations further weakens interlayer magnetic interactions, confining these interactions within the two-dimensional layers. This effectively suppresses the formation of long-range magnetic order. This confirms that under the test conditions, Cu^{2+} in $ETPCuCl_3$ crystals exhibits paramagnetic behaviour, rather than ordered magnetic states, such as ferromagnetism or antiferromagnetism, which possess hysteresis characteristics.[35,36]

This result elucidates the regulation of "valence–structure–function" in copper-based OIPT through analysis of the $ETPCuCl_2$ to $ETPCuCl_3$ oxidation phase transformations. Its core lies in the valence transition from Cu^{+} (d^{10}) to Cu^{2+} (d^9). This fundamental electronic change not only generates apparent magnetism due to the presence of unpaired electrons, but also drives crystal structural reconstruction. Subsequently, through super-exchange interactions, it enables a functional switch from nonlinear optics to magnetism. This mechanism is clearly elucidated in copper-based systems: modulating d-orbital electrons *via* valence state changes to achieve macroscopic properties. Similar valence control principles are observed in other metallic systems (*e.g.*, Ni^{3+}/Ni^{4+}, Ti^{3+}/Ti^{4+}, Sn^{2+}/Sn^{4+}),[3–5,37] indicating that oxidation-induced valence transitions represent a universal strategy for optimizing functional material properties.

In summary, we successfully synthesized $ETPCuCl_2$ single crystals *via* the slow evaporation method and observed for the first time their oxidation-induced crystal phase transformation behavior. The core issue of this process lies in the valence state transformation of cuprous cations (Cu^{+}) in $ETPCuCl_2$ being oxidized into copper ions (Cu^{2+}), which directly triggers the reconstruction of the centrosymmetric crystal structure of $ETPCuCl_3$. Moreover, this process facilitates a remarkable

functional transition in the material, shifting from second harmonic generation response to magnetic properties. This work not only reveals the intrinsic "valence–structure–property" correlation mechanism underlying oxidation-induced phase transformations, enriching the design theory of multifunctional materials, but also lays a crucial foundation for developing a new generation of magnetic materials with switchable functionalities.

Author contributions

Mengjie Sang: investigation, writing – original draft and data curation. Yanqing Liu: writing – review & editing, supervision and funding acquisition. Guokui Liu: investigation, formal analysis, methodology, software and data curation. Yangyang Dang: writing – review & editing, project administration, supervision, conceptualization and funding acquisition.

Conflicts of interest

All the authors declare no conflict of interest.

Data availability

The data that support the findings of this study are available from the corresponding author upon reasonable request.

Supplementary information (SI): experimental section, XPS and crystal data. See DOI: https://doi.org/10.1039/d5dt02573g.

CCDC 2497620 and 2497621 contain the supplementary crystallographic data for this paper.[38a,b]

Acknowledgements

This work was supported by the Natural Science Foundation of Shandong Province (No. ZR2023ME095 and ZR2022MA067). All the authors thank Dr Chunlong Li (Qilu University of Technology), Dr Jing Wei (Beijing Institute of Technology) and Prof. Qi Wu (Wuhan Textile University) for their help in UV-vis spectra, XPS and NLO measurements.

References

1 X. Zhao, J. Li, W. Li, P. Lu, X. Zhang, X. Zhao, Y. Xu, M. Xia and J. Tang, Valence state regulation of Terbium in all-inorganic amorphous solid for magnetic field sensing, *Chem. Eng. J.*, 2024, **488**, 150898.

2 J. Yang, L. X. Song, J. Yang, Z. Dang and J. Chen, A controllable transformation in copper valence states and its applications, *Dalton Trans.*, 2012, **41**, 2393.

3 Y. Li, Y. Yang, X. Shu, D. Wan, N. Wei, X. Yu, M. B. H. Breese, T. Venkatesan, J. M. Xue, Y. Liu, S. Li, T. Wu and J. Chen, From titanium sesquioxide to titanium dioxide: oxidation-induced structural, phase, and property evolution, *Chem. Mater.*, 2018, **30**, 4383.

4 G. Teri, H.-F. Ni, Q.-F. Luo, X.-P. Wang, J.-Q. Wang, D.-W. Fu and Q. Guo, Tin-based organic-inorganic metal halides with a reversible phase transition and thermochromic response, *Mater. Chem. Front.*, 2023, **7**, 2235.

5 B. Yu, C. Yang, Z. Song, G. Liu, J. Wei, Q. Wu and Y. Dang, Oxidation-induced phase transformations of hybrid tin bromide single crystals enable the occurrence of second-harmonic generation, *Inorg. Chem. Front.*, 2023, **10**, 535.

6 A. Y. Madkhli, Simultaneous oxidation of Mn^{2+} to Mn^{4+} by devitrification of transparent glassy $Na_2Ge_4O_9$: Mn, *Ceram. Int.*, 2024, **50**, 24913.

7 A. Kultaeva, T. Biktagirov, P. Neugebauer, H. Bamberger, J. Bergmann, J. Van Slageren, H. Krautscheid and A. Pöppl, Multifrequency EPR, SQUID, and DFT study of cupric ions and their magnetic coupling in the metal-organic framework compound $_\infty^3$[Cu(prz-trz-ia)], *J. Phys. Chem. C*, 2018, **122**, 26642.

8 Y. Li, H. Cheng, Z. Alhalili, G. Xu and G. Gao, The progress of magnetic sensor applied in biomedicine: A review of non-invasive techniques and sensors, *J. Chin. Chem. Soc.*, 2021, **68**, 216.

9 Q. Zhang, J. Song, Z. Wu, L. Hu, S. Li and S. Sang, A flexible magnetic field sensor based on paramagnetic C_{60}@Fe_3O_4 nanocomposites and ordered hexagonally structured substrate, *J. Magn. Magn. Mater.*, 2021, **537**, 168171.

10 R. E. P. Winpenny, Quantum Information Processing Using Molecular Nanomagnets As Qubits, *Angew. Chem., Int. Ed.*, 2008, **47**, 7992.

11 E. Cisternas, E. E. Vogel and J. Faúndez, Stability of bar code information stored in magnetic nanowire arrays, *Adv. Condens. Matter Phys.*, 2017, **2017**, 1.

12 M. Kumar, A. Kumar, A. Singh, A. Anshul, S. Sharma and P. C. Sati, Low temperature magnetic study and first principle calculation in 'Mo' doped $CoFe_2O_4$ for magnetic information storage applications, *J. Alloys Compd.*, 2022, **896**, 163074.

13 N. J. Harmon and D. O. Kumi, Phenomenological modeling of electron-hole recombination in promising photocatalytic magnetic materials, *J. Phys. Chem. Lett.*, 2025, **16**, 2181.

14 M. J. Jacinto, L. F. Ferreira and V. C. Silva, Magnetic materials for photocatalytic applications-a review, *J. Sol-Gel Sci. Technol.*, 2020, **96**, 1.

15 J. Chen, Z. Cai, S. Jiao, X. Zhang, J. Hu, M. Liu, B. Sun and X. Hua, A thermally responsive dielectric switchable zero-dimensional organic-inorganic hybrid material: $(C_3H_6NH_2)_2CoCl_4$, *Acta Chim. Sin.*, 2023, **81**, 480.

16 C. Zhou, H. Lin, S. Lee, M. Chaaban and B. Ma, Organic-inorganic metal halide hybrids beyond perovskites, *Mater. Res. Lett.*, 2018, **6**, 552.

17 Y. Bai, Z. Yang, Q. Deng, H. Zan, S. Cao, X. Han, M. Yuan, T. Chang and R. Zeng, Enhanced nonlinear optical response and self-powered CPL detection in unique triangular-tetrahedral chiral copper(I) halides, *Angew. Chem., Int. Ed.*, 2025, **64**, e202509283.

18 F. Ge, B. Li, P. Cheng, G. Li, Z. Ren, J. Xu and X. Bu, Chiral hybrid copper(I) halides for high efficiency second harmonic generation with a broadband transparency window, *Angew. Chem., Int. Ed.*, 2022, **61**, e202115024.
19 Z. Guo, J. Li, J. Liang, C. Wang, X. Zhu and T. He, Regulating optical activity and anisotropic second-harmonic generation in zero-dimensional hybrid copper halides, *Nano Lett.*, 2022, **22**, 846.
20 S. Dutta, D. Vishnu, S. K. S. Som, R. Chaurasiya, D. K. Patel, K. Moovendaran, C.-C. Lin, C.-W. Chen and R. Sankar, Segmented highly reversible thermochromic layered perovskite $[(CH_2)_2(NH_3)_2]CuCl_4$ crystal coupled with an inverse magnetocaloric effect, *ACS Appl. Electron. Mater.*, 2022, **4**, 521.
21 C. Han, A. J. Bradford, A. M. Z. Slawin, B. E. Bode, E. Fusco, S. L. Lee, C. C. Tang and P. Lightfoot, Structural features in some layered hybrid copper chloride perovskites: $ACuCl_4$ or A_2CuCl_4, *Inorg. Chem.*, 2021, **60**, 11014.
22 M. A. Halcrow, Jahn-Teller distortions in transition metal compounds, and their importance in functional molecular and inorganic materials, *Chem. Soc. Rev.*, 2013, **42**, 1784–1795.
23 J. Liu, H.-J. Koo, H. Xiang, R. K. Kremer and M.-H. Whangbo, Most spin-1/2 transition-metal ions do have single ion anisotropy, *J. Chem. Phys.*, 2014, **141**, 124113.
24 M. Yang, W.-D. Yao, W. Liu and S.-P. Guo, The first quaternary rare-earth oxythiogermanate with second-harmonic generation and ferromagnetic behavior, *Chem. Commun.*, 2023, **59**, 3894.
25 X. Han, P. Cheng, W. Han, R. Shi, J. Guan, G. Li and J. Xu, Circularly polarized luminescence and nonlinear optical harmonic generation based on chiral zinc halides, *Chem. Commun.*, 2023, **59**, 7447.
26 J. Yang, L. X. Song, J. Yang, Z. Dang and J. Chen, A controllable transformation in copper valence states and its applications, *Dalton Trans.*, 2012, **41**, 2393.
27 M. M. Roessler and E. Salvadori, Principles and applications of EPR spectroscopy in the chemical sciences, *Chem. Soc. Rev.*, 2018, **47**, 2534.
28 A. Ambreen, Q. You, N. Xia, N. Yan and Z. Wu, Nonstoichiometric and ligand-dependent paramagnetism of $Au_{24}Cd(SR)_{18}$ nanoclusters, *Sci. China Mater.*, 2023, **66**, 4886.
29 I. Caretti, B. Dervaux, F. E. Du Prez and S. Van Doorslaer, The nature of Cu(II) species in ATRP: new insights via EPR, *J. Polym. Sci., Part A:Polym. Chem.*, 2010, **48**, 1493.
30 Y. Yerli, EPR studies of Cu^{2+} in tetraaqua-di(nicotinamide) Zn(II)-saccharinate single crystals, *Spectrochim. Acta, Part A*, 2007, **66**, 1288.
31 X.-H. Chen, R.-Z. Guo, Y.-X. Huang, Y. Pan and J.-X. Mi, Crystal structure and magnetic properties of the magnetically isolated zigzag chain in $KGaCu(PO_4)_2$, *Dalton Trans.*, 2021, **50**, 7835.
32 A. Hassanpoor, M. Mirzaei, M. N. Shahrak and A. M. Majcher, Developing a magnetic metal organic framework of copper bearing a mixed azido/butane-1,4- dicarboxylate bridge: magnetic and gas adsorption properties, *Dalton Trans.*, 2018, **47**, 13849.
33 M. M. Turnbull, C. P. Bedford, R. L. Forman, C. P. Landee, D. A. Dickie and J. L. Wikaira, The two-halide super exchange pathway in Cu(II) chains: synthesis, structure, and magnetic behavior of (2-X-3-methylpyridinium)$_2$ [CuX'$_4$] (X, X' = Cl, Br), *J. Coord. Chem.*, 2025, **78**, 2037.
34 N. Sun, L. Sun, Y. Yu, Z. Peng, S. Du and Z. Liu, Synthesis, Crystal Structure, and Properties of a Pair of 3D Chiral Cu (II) Coordination Polymer Enantiomers Based on 5-(1-Carboxyethoxy) Isophthalic Acid, *ACS Omega*, 2025, **10**, 11168.
35 N. Jiang, S. Velliyarat, C.-Y. Lien, H. L. Nguyen, J. Hofmann, J.-H. Chen, A. Ramanathan, A. S. Filatov, H. S. L. Pierre, S. Patel, K. W. Chapman, J.-N. Boyn and J. S. Anderson, Pre-synthetic redox control of structure and properties in copper TTFtt coordination polymers, *Chem. Sci.*, 2025, **16**, 19304.
36 J. C. R. Aquino, F. H. Aragón, J. A. H. Coaquira, X. Gratens, V. A. Chitta, I. Gonzales, W. A. A. Macedo and P. C. Morais, Evidence of Cr^{3+} and Cr^{4+} coexistence in chromium-doped SnO_2 nanoparticles: A structural and magnetic study, *J. Phys. Chem. C*, 2017, **121**, 21670.
37 Q. Ding, Z. Shen, S. Xiang, H. Tian, J. Li and Z. Zhang, *In situ* environmental TEM study of γ'-γ phase transformation induced by oxidation in a nickel-based single crystal superalloy, *J. Alloys Compd.*, 2015, **651**, 255.
38 (*a*) CCDC 2497620: Experimental Crystal Structure Determination, 2025, DOI: 10.5517/ccdc.csd.cc2ptzdx; (*b*) CCDC 2497621: Experimental Crystal Structure Determination, 2025, DOI: 10.5517/ccdc.csd.cc2ptzfy.